Inorganic Chemistry

Article

pubs.acs.org/IC

Exploring a New Structure Family: Alkali Borosulfates $Na_5[B(SO_4)_4]$, $A_3[B(SO_4)_3]$ (A = K, Rb), $Li[B(SO_4)_2]$, and $Li[B(S_2O_7)_2]$

Michael Daub,[†] Karolina Kazmierczak,[‡] Peter Gross,[‡] Henning Höppe,*[,‡] and Harald Hillebrecht*[,†,§]

[†]Institut für Anorganische und Analytische Chemie, Albert-Ludwigs-Universität, Albertstraße 21, D-79104 Freiburg, Germany

[‡]Institut für Physik, Universität Augsburg, Universitätsstraße 1, D-86159 Augsburg, Germany

[§]Freiburger Materialforschungszentrum FMF, Albert-Ludwigs-Universität, Stefan-Meier-Straße 25, D-79104 Freiburg, Germany

Supporting Information

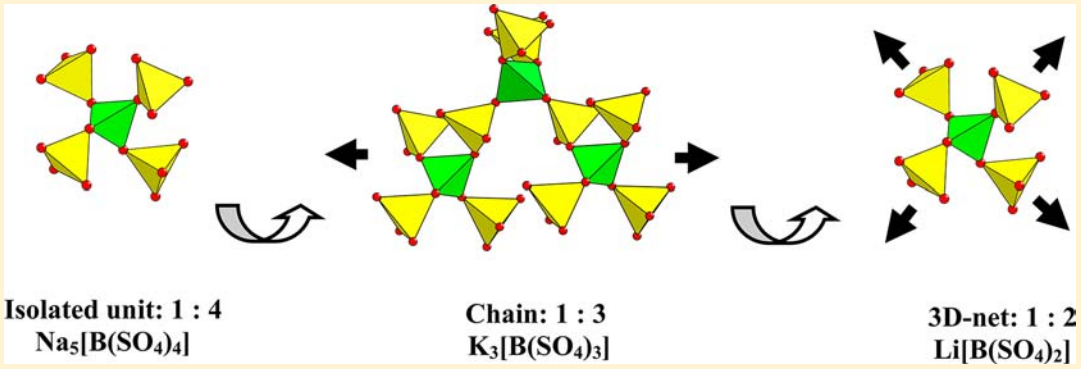

ABSTRACT: New alkali borosulfates were obtained by precipitation from oleum, solid-state reactions, or thermal decomposition. The crystal structures were characterized with single-crystal data. They are all based on corner-linked BO_4 and SO_4 tetrahedra with varying coordination of the alkali cations. According to the ratio of BO_4 and SO_4 tetrahedra, different frameworks are observed, i.e., noncondensed complex anions (1:4), one-dimensional chains (1:3), or three-dimensional (3D) networks (1:2). This is in analogy to silicates, where the ratio Si/O relates to the dimensionality also. For $Na_5[B(SO_4)_4]$, which exists in two different polymorphs, there are noncondensed pentameric units. $Na_5[B(SO_4)_4]$-I: space group $Pca2_1$, a = 10.730(2) Å, b = 13.891(3) Å, c = 18.197(4) Å. $Na_5[B(SO_4)_4]$-II: space group $P2_12_12_1$, a = 8.624(2) Å, b = 9.275(2) Å, c = 16.671(3) Å. $A_3[B(SO_4)_3]$ (A = K, Rb) are isotypic with $Ba_3[B(PO_4)_3]$ adopting space group $Ibca$ [$K_3[B(SO_4)_3]$, a = 7.074(4) Å, b = 14.266(9) Å, c = 22.578(14) Å; $Rb_3[B(SO_4)_3]$, a = 7.2759(5) Å, b = 14.7936(11) Å, c = 22.637(2) Å] with vierer chains of BO_4 tetrahedra based on two bridging and two terminal SO_4 tetrahedra. $Li[B(SO_4)_2]$ [space group Pc, a = 7.6353(15) Å, b = 9.342(2) Å, c = 8.432(2) Å, and β = 92.55(2)°] comprises a 3D network that is closely related to β-tridymite. $Li[B(S_2O_7)_2]$ [space group $P2_12_12_1$, a = 10.862(2) Å, b = 10.877(2) Å, c = 17.769(4) Å] represents the first example of a disulfate complex with noncondensed $[B(S_2O_7)_2]^-$ units. Vibrational spectra were recorded from all compounds, and the thermal behavior was also investigated.

1. INTRODUCTION

Recently, we reported on $K_5[B(SO_4)_4]$ as the first example for a borosulfate.[1] The interest in this new class of compounds arises for two reasons. On the one hand, the exploitation of a new class of compounds is one of the most exciting challenges for basic research in the field of synthetic chemistry. So, one goal is the search for experimental methods to gain access to new representatives. Furthermore, these results extend our knowledge on crystal chemical relations as well as systematics and may provide access to novel exciting structure motifs. On the other hand, compounds with oxidic framework structures comprising tetrahedra and thus favoring noncentrosymmetric crystal structures are promising candidates for new optical materials.[2−8] Using the high structural variability of multinary oxides and understanding the underlying structure−property relationships may allow one to develop cheap and/or highly efficient optical materials for many applications such as luminescence, up/down conversion, or nonlinear optics.[6]

$K_5[B(SO_4)_4]$ represents the starting point for our considerations. A first aspect gives attention to the structural classification. The structure of $K_5[B(SO_4)_4]$ shows a similarity to silicates[7] and borophosphates[8] according to the topology of corner-linked tetrahedra. We assumed that the resulting framework of tetrahedra depends on the ratio of BO_4/SO_4 and on the size and number of additional cations between the tetrahedral framework. For a ratio of 1:4, the formation of isolated tetrahedral units similar to orthosilicates with isolated SiO_4^{4-} tetrahedra is evident. In analogy to silicates, we expected chain structures for a ratio of 1:3 (SiO_3^{2-}) and a three-dimensional (3D) network structure for a ratio of 1:2 (SiO_2). Finally, similar structures for borosulfates $A_m[B(SO_4)_n]$ and borophosphates $EA_m[B(PO_4)_n]$ with suitable charge and size of the cation may result. Our recent

Received: February 11, 2013
Published: May 8, 2013

   dx.doi.org/10.1021/ic400267s | Inorg. Chem. 2013, 52, 6011−6020

results on new borosulfates impressively confirm these expectations, but also some unexpected features result.

A second aspect deals with synthetic access to borosulfates. In principle, there are several ways. Besides a simple stoichiometric solid-state synthesis, for example, $ABO_2 + 2A_2S_2O_7 \rightarrow A_5B(SO_4)_4$, or precipitation from less or more concentrated sulfuric acid, there are a great number of promising thermal decomposition reactions such as the loss of H_2O and/or SO_3 from H_2SO_4, H_3BO_3, $AHSO_4$, A_2SO_4, etc., that lead to borosulfates. Especially, the recent work of Wickleder et al.[9,10] has shown the great influence of the experimental conditions. The results presented in this contribution give a glance into versatile ways leading to the exciting new world of borosulfates.

2. EXPERIMENTAL SECTION

2.1. Synthesis. *$K_3[B(SO_4)_3]$.* The synthesis was performed according to eq 1, starting from stoichiometric amounts of potassium disulfate and boron oxide.

$$3K_2S_2O_7 + B_2O_3 \rightarrow 2K_3[B(SO_4)_3] \quad (1)$$

A mixture of 761.8 mg (3.0 mmol) of potassium disulfate $K_2S_2O_7$ (Grüssing, 99%) and 69.9 mg (1.0 mmol) of boron oxide B_2O_3 (ABCR, 99.6%) was transferred into a silica crucible. The latter was heated under an ambient atmosphere to 673 K at a rate of 60 K/h and cooled to room temperature at a rate of 30 K/h. $K_3[B(SO_4)_3]$ was obtained quantitatively as a phase-pure crystalline, colorless, and slightly hygroscopic powder. Experimental and calculated X-ray diffraction (XRD) patterns are shown in the Supporting Information (SI).

$K_5[B(SO_4)_4]$. The synthesis and crystal growth of $K_5[B(SO_4)_4]$ were already described.[1] Now we have obtained single crystals of superior quality by thermal decomposition of $K_3[B(SO_4)_3]$ according to eq 2 upon maintaining the reaction mixture at 673 K for 12 h.

$$5K_3[B(SO_4)_3] \rightarrow 3K_5[B(SO_4)_4] + B_2O_3 + SO_3\uparrow \quad (2)$$

The powder XRD (see Supporting Information) showed only reflections of $K_5[B(SO_4)_4]$. B_2O_3 was not detected because it is probably amorphous. This can explain the broad background between 10 and 15° (2θ).

$Rb_3[B(SO_4)_3]$. A total of 35.0 mg (1.0 mmol) of boron oxide B_2O_3 (ABCR, 99.6%) and 179.5 mg (1.5 mmol) of RbCl (Merk, 99.99%) were added to 1.0 mL of concentrated sulfuric acid H_2SO_4 (VWR, normapur, 95%) in a silica crucible and heated under air to 673 K for 20 h. Cl^- leaves as gaseous HCl. Crystals of $Rb_3[B(SO_4)_3]$ were formed as colorless platelets. $Rb_3[B(SO_4)_3]$ could not be obtained phase-purely; we always obtained microcrystalline $RbHSO_4$[11] as a second phase. According to characterization by powder XRD (see the SI), the amounts are nearly equal.

$Na_5[B(SO_4)_4]$-I. The synthesis was performed according to eq 3, starting from sodium hydrogen sulfate hydrate and boric acid.

$$5NaHSO_4\cdot H_2O + B(OH_3) \rightarrow Na_5[B(SO_4)_4] + SO_3\uparrow + 9H_2O\uparrow \quad (3)$$

A mixture of 689.8 mg (4.996 mmol) of sodium hydrogen sulfate hydrate $NaHSO_4\cdot H_2O$ (Fa. Grüssing, 99%) and 62.0 mg (1.00 mmol) of boric acid $B(OH)_3$ (Fa. Grüssing, 99%) was transferred into a silica crucible. Then it was heated to 673 K at a rate of 30 K/h. After 12 h, the mixture was cooled to room temperature at a rate of 5 K/h. $Na_5[B(SO_4)_4]$-I was obtained quantitatively as a crystalline, colorless, and slightly hygroscopic powder (for XRD patterns, see the SI).

$Na_5[B(SO_4)_4]$-II. A few colorless single crystals of $Na_5[B(SO_4)_4]$-II were obtained as byproducts during the synthesis of $Na_5[B(SO_4)_4]$-I at 623 K at a cooling rate of 60 K/h. All attempts to synthesize significant amounts of $Na_5[B(SO_4)_4]$-II failed, so the characterization is based solely on the single-crystal data. XRD patterns have never shown reflections of $Na_5[B(SO_4)_4]$-II (see the SI).

$Li[B(S_2O_7)_2]$. The synthesis was performed according to eq 4, starting from lithium sulfate hydrate, boron oxide, and oleum.

$$8H_2S_2O_7 + B_2O_3 + Li_2SO_4\cdot H_2O \rightarrow 2Li[B(S_2O_7)_2] + 9H_2SO_4 \quad (4)$$

A total of 10 mL of oleum (Merck, 65% SO_3) was added to a mixture of 1.4 g (11 mmol) of lithium sulfate hydrate $Li_2SO_4\cdot H_2O$ (VWR/Merck, 99%) and 1.4 g (20 mmol) of boron oxide B_2O_3 (ABCR, 99.6%). After 1 week, the precipitate was sucked off under vacuum. $Li[B(S_2O_7)_2]$ was obtained as a phase-pure crystalline, colorless, and extremely moisture-sensitive powder (for experimental and calculated XRD patterns, see the SI). Again, an amorphous byproduct occurs, probably B_2O_3.

$Li[B(SO_4)_2]$. The synthesis was performed by thermal decomposition according to eq 5, starting from $Li[B(S_2O_7)_2]$.

$$Li[B(S_2O_7)_2] \rightarrow Li[B(SO_4)_2] + 2SO_3\uparrow \quad (5)$$

A sample of $Li[B(S_2O_7)_2]$ was heated in a silica crucible in air to 573 K at a rate of 60 K/h. After 12 h, the mixture was cooled to room temperature at a rate of 60 K/h. $Li[B(SO_4)_2]$ was obtained quantitatively as a phase-pure crystalline, colorless, and hygroscopic powder (for experimental and theoretical XRD patterns, see the SI).

2.2. Vibrational Spectroscopy. Raman spectra were recorded by a Bruker FRA 106/S module with a Nd:YAG laser (λ = 1064 nm) in a scanning range from 400 to 4000 cm^{-1}. IR spectra were recorded on a Nicolet Magna 760 spectrometer using a Diamond Orbit ATR unit (extended ATR correction with a refraction index of 1.5 was used).

2.3. Thermal Analysis. Thermogravimetric (TG) and differential thermal (DTA) analyses were carried out in a silica glass sample holder using a simultaneous thermoanalysis apparatus STA429 (Netzsch) under argon (heating rate, 2 K/min; flow rate, 200 mL/min) in the range from room temperature to 1150 K.

2.4. Crystal Structure Determination and Refinement. All single crystals were handled in an argon-filled glovebox and enclosed in a silica glass capillary for measurements. XRD data of single crystals were collected on a Stoe IPDS II area detection diffractometer (room temperature data) and a Bruker Quazar/APEX II (low-temperature data) with a CCD detector using Mo Kα radiation (λ = 0.710 73 Å, graphite monochromated). The raw data were processed and corrected numerically for absorption using software of the respective supplier.[12−14] Crystal structures were solved by direct methods and refined by full matrix least squares refinements on F^2 by *SHELXTL*.[15] In all cases, refinements were performed with anisotropic displacement parameters for all atoms. Noncentrosymmetric structures were checked for the correct symmetry by *MISSYM/PLATON*.[16] With the exception of $A_3[B(SO_4)_3]$ (A = K, Rb), all crystal structures represent new structure types.

The crystal structure of $Na_5[B(SO_4)_4]$-I was finally refined in space group $Pca2_1$ (No. 29). The initial structure solution, also in space group $Pca2_1$, was based on a smaller unit cell with $a' = {}^1/_2a$ and yielded two sodium atoms spread across split positions. According to the diffraction pattern, a weak superstructure was identified, leading to a doubled a axis. In this model, all atoms could be localized with sound displacement parameters on fully occupied sites. The crystal structure (see below) confirms these findings unequivocally.

As was already mentioned, we obtained only a few crystals of $Na_5[B(SO_4)_4]$-II, so characterization is based only on the single-crystal data. The crystal structure of $Na_5[B(SO_4)_4]$-II was solved and refined in space group $P2_12_12_1$ (No. 19). The investigated crystal was a nonmerohedral twin. This might explain the slightly higher residuals.

The structures of $A_3[B(SO_4)_3]$ (A = K, Rb) are isotypic and were solved and refined in space group *Ibca* (No. 73) without peculiarities. Later on, it turned out that both compounds belong to the $Ba_3[B(PO_4)_3]$ structure type.[17]

Refinement of $K_5[B(SO_4)_4]$ was done using our known model,[1] which was confirmed with significantly smaller standard deviations.

$Li[B(SO_4)_2]$ crystallizes monoclinically in space group *Pc* (No. 7) with a = 7.6353(15) Å, b = 9.342(2) Å, c = 8.432(2) Å, and β = 92.57(3)°. The crystal structure was solved and refined without peculiarities.

The first measurement of $Li[B(S_2O_7)_2]$ was done at room temperature and resulted in a tetragonal unit cell with a = 10.9070(15) Å and c = 17.848(4) Å. According to the Laue class, reflection conditions, and E

dx.doi.org/10.1021/ic400267s | Inorg. Chem. 2013, 52, 6011−6020

statistics, the structure solution was initially performed in space group $P4_12_12$. The subsequent refinement yielded a reasonable structure model and satisfying R values of R1 = 0.034 and wR2 = 0.055, but some of the oxygen atoms showed enlarged displacement parameters, which seemed to be caused by disorder/twinning. Therefore, the measurement was repeated at 150 K. It turned out that at low temperatures the true unit cell is orthorhombic, with a = 10.862(2) Å, b = 10.877(2) Å, and c = 17.769(4) Å adopting space group $P2_12_12_1$ (No. 19). Furthermore, the crystal is pseudomerohedrally twinned because of the pseudotetragonal metrics ($a \approx b$) and the assumed phase transition from tetragonal to orthorhombic.

Table 1 shows data for the structure refinements of single crystals. Tables 2–4 give selected distances and angles. Coordinates and displacement parameters are listed in the SI. Further details of the crystal structure investigations presented in this work may be obtained from the Fachinformationszentrum Karlsruhe, D-76344 Eggenstein-Leopoldshafen, Germany (e-mail: crysdata@fiz-karlsruhe.de) upon quoting the depository numbers CSD-425172 ($K_3[B(SO_4)_3]$), CSD-425178 ($Rb_3[B(SO_4)_3]$), CSD-425176 ($Na_5[B(SO_4)_4]$-I), CSD-425177 ($Na_5[B(SO_4)_4]$-II), CSD-425173 ($K_5[B(SO_4)_4]$), CSD-425174 ($Li[B(SO_4)_2]$), and CSD-415175 ($Li[B(S_2O_7)_2]$), the names of the authors, and citation of this publication.

All samples were checked for identity and purity by recording XRD patterns of powdered samples. The experimental data were compared to theoretical patterns obtained from the single-crystal data. For the measurements, powdered samples were enclosed in a glass capillary with 0.3 mm diameter and investigated at room temperature in Debye–Scherrer geometry on a STOE Stadi P powder diffractometer with Ge(111)-monochromatized Mo Kα radiation (linear PSD detector, step width 0.5°, and acquisition time 200 s/step).

3. RESULTS AND DISCUSSION

3.1. Crystal Structures. *$Na_5[B(SO_4)_4]$-I and $Na_5[B(SO_4)_4]$-II.* $Na_5[B(SO_4)_4]$ crystallizes in two modifications, which both represent new structure types. According to the ratio B/S of 1:4, the crystal structure of $Na_5[B(SO_4)_4]$ comprises condensed sulfate and borate tetrahedra. Similar to $K_5[B(SO_4)_4]$, they form an open-branched pentameric anion with the borate tetrahedron in the center (Figure 1) and the sodium cations between these units. The difference between the two forms is the arrangement of the pentamers and the surrounding of Na^+, while the units themselves are quite similar.

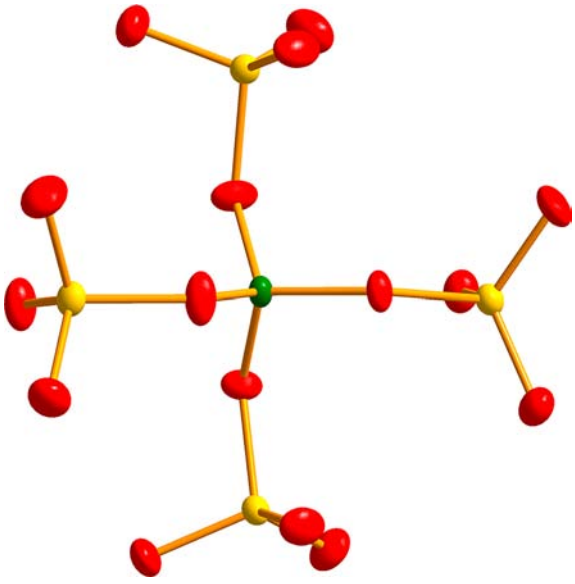

Figure 1. Borosulfate anion in $Na_5[B(SO_4)_4]$-I. Color code: B, green; S, yellow; O, red. Thermal ellipsoids are set to 50% probability.

In modification I, the pentamers are stacked one above the other along [100], forming a hexagonal rod packing (Figure 2a). Viewed along [010], they are arranged in corrugated layers (Figure 2b). The projections show the subcell with $a' = {}^1/_2a$ (see the structure solution). The arrangement in modification II is more isotropic (Figure 3) and closer to a *bcc* packing, as was found in $K_5[B(SO_4)_4]$ (Figure 4).

Because of its similarity, the geometry of the pentamers will be discussed together for both forms (data for modification II in italics; figures in the SI). As expected and also observed for $K_5[B(SO_4)_4]$, the bonds from the sulfur atoms to the bridging oxygen atoms O^{br} are significantly longer compared with those to the terminal oxygen atoms O^{term}. The bond lengths S–O^{term} range from 1.43 to 1.46 Å (*1.40–1.46 Å*), thus being shorter than the bond lengths S–O^{br} (1.54–1.58 Å; *1.53–1.59 Å*). The angles O^{br}–S–O^{term} (103–110°, *101–109°*) are smaller compared to the angles O^{term}–S–O^{term} (109–115°; *110–115°*). They agree well with typical bond lengths and angles inside other condensed (boro)sulfates.[1,9,10] The bond lengths in the BO_4 tetrahedron range from 1.44 to 1.51 Å (*1.45–1.49 Å*).

We have already applied measurements for the deviations of tetrahedra from the ideal symmetry suggested by Balic-Žunic and Makovicky,[18,19] for example, to polyphosphates such as β-$Ln(PO_3)_3$ (Ln = Sc, Y, Tb–Yb).[20] For these, we identified typical values for condensed phosphate tetrahedra of less than 1%. The deviations from ideal symmetry gave values in the range from 1.22 to 1.32% (*0.46%*) for the borate and from 0.07 to 0.22% (*0.10–0.35%*) for the sulfate tetrahedra. Apparently, the deviation is lower with higher formal charge of the central atom; therefore, the criterion for regular tetrahedra derived from phosphates(V) may be too strict for borate(III) tetrahedra. While for the sulfate tetrahedra in $Na_5[B(SO_4)_4]$-II all values are well below this value and may be classified as regular, the borate tetrahedra in $Na_5[B(SO_4)_4]$-I are slightly above. In general, the geometry of the pentamers in $Na_5[B(SO_4)_4]$ is very similar to that in $K_5[B(SO_4)_4]$. Once more, these results confirm our experience[19] that tetrahedra show fewer distortions with increasing charge of the central atom.

According to the different arrangements of the pentamers, the surroundings of the sodium atoms are different. In modification I, the 10 crystallographically different sodium atoms show rather different coordination spheres by oxygen. Na–O distances are found between 2.26 and 2.99 Å. This distance range agrees well with the sum of the ionic radii; that is, 2.56 Å (CN = 8), 2.53 Å (CN = 7), 2.42 Å (CN = 6), and 2.40 Å(CN = 5) for Na^+ and O^{2-}.[21] Most are 6-fold (Na1, Na2, Na4, Na5, and Na8), some are 7-fold (Na3 and Na9) and 8-fold (Na6 and Na7), and only one is 5-fold-coordinated (Na10). Nevertheless, the sum of the bond valence[22] is very similar in the range between 1.21 (Na4) and 1.40 (Na2).

In modification II, three sodium atoms are 6-fold (Na1, Na3, and Na5) and two are 7-fold-coordinated (Na2 and Na4) by oxygen in a range from 2.26 to 2.99 Å. The valence sum spans from 1.08 (Na2) to 1.43 (Na1), which is broader than that in modification I and might explain the dominance of form I. On the other hand, there are more distorted BO_4 tetrahedra in modification I than in modification II.

$A_3[B(SO_4)_3]$ (A = K, Rb). Both compounds crystallize isotypically to $Ba_3[B(PO_4)_3]$.[17] The crystal structure contains condensed sulfate and borate tetrahedra, forming an open-branched vierer single chain (Figure 4). These borosulfate chains are running zigzag-shaped parallel [010] with two terminal and two bridging sulfate anions. Between these polymeric chains are

dx.doi.org/10.1021/ic400267s | Inorg. Chem. 2013, 52, 6011–6020

Table 1. Crystallographic Data of $A_5[B(SO_4)_4]$ (A = Na, K), $A_3[B(SO_4)_3]$ (A = K, Rb), $Li[B(SO_4)_2]$, and $Li[B(S_2O_7)_2]$ (Estimated Standard Deviations in Parentheses)

	$K_3[B(SO_4)_3]$	$Rb_3[B(SO_4)_3]$	$Na_5[B(SO_4)_4]$-I	$Na_5[B(SO_4)_4]$-II	$K_5[B(SO_4)_4]$	$Li[B(SO_4)_2]$	$Li[B(S_2O_7)_2]$
Temperature (K)	293(2)	293(2)	293(2)	293(2)	293(2)	150(2)	150(2)
cryst shape	platelet	platelet	platelet	platelet	platelet	irregular polyhedron	irregular polyhedron
color	colorless	colorless	colorless	colorless	colorless	colorless	colorless
size (mm^3)	0.55 × 0.20 × 0.01	0.27 × 0.09 × 0.02	0.2 × 0.045 × 0.03	0.15 × 0.05 × 0.02	0.20 × 0.08 × 0.02	0.25 × 0.10 × 0.05	0.25 × 0.10 × 0.05
cryst syst	orthorhombic	orthorhombic	orthorhombic	orthorhombic	tetragonal	monoclinic	orthorhombic
space group	*Ibca*	*Ibca*	$Pca2_1$	$P2_12_12_1$	$P4_1$	*Pc*	$P2_12_12_1$
unit cell dimens							
a (Å)	7.074(4)	7.2759(5)	10.730(2)	8.6239(17)	9.9044(14)	7.6353(15)	10.863(2)
b (Å)	14.266(9)	14.7936(11)	13.891(3)	9.2750(19)		9.342(2)	10.877(2)
c (Å)	22.578(14)	22.637(2)	18.197(4)	16.671(3)	16.215(3)	8.432(2)	17.769(4)
β (deg)						92.55(2)	
Z	8	8	8	4	4	4	8
d_{calcd} (g/cm^3)	2.427	3.028	2.498	2.540	2.466	2.320	2.341
data collection	STOE IPDS II[12]	STOE IPDS II[12]	STOE IPDS II[12]	STOE IPDS II[12]	STOE IPDS II[12]	STOE IPDS II[12]	Bruker Quazar/APEX II[13]
	Mo Kα; λ = 0.71073 Å (graphite monochromated)	Mo Kα; λ = 0.71073 Å (graphite monochromated)	Mo Kα; λ = 0.71073 Å (graphite monochromated)	Mo Kα; λ = 0.71073 Å (graphite monochromated)	Mo Kα; λ = 0.71073 Å (graphite monochromated)	Mo Kα; λ = 0.71073 Å (graphite monochromated)	Mo Kα; λ = 0.71073 Å (graphite monochromated)
	$0° \le \omega \le 180°$	$0° \le \omega \le 180°$	$0° \le \omega \le 180°$	$0° \le \omega \le 180°$	$0° \le \omega \le 180°$	$0° \le \omega \le 180°$	12 scans
	ψ = 0°; $\Delta\omega$ = 1°	ψ = 0°; $\Delta\omega$ = 1°	ψ = 0°; $\Delta\omega$ = 1°	ψ = 0°; $\Delta\omega$ = 1°	ψ = 0°; $\Delta\omega$ = 1°	ψ = 0°; $\Delta\omega$ = 1°	2334 frames
exposure time (s)	240	180	120	120	120	60	20
2θ range (deg)	50	50	58.6	50	50	58.3	50
index ranges	$-8 < h < 8$; $-16 < k < 16$; $-26 < l < 26$	$-8 < h < 8$; $-17 < k < 17$; $-26 < l < 26$	$-14 < h < 14$; $-19 < k < 19$; $-24 < l < 24$	$-8 < h < 10$; $-10 < k < 10$; $-19 < l < 19$	$-11 < h < 11$; $-11 < k < 11$; $-19 < l < 19$	$-10 < h < 10$; $-12 < k < 11$; $-11 < l < 11$	$-12 < h < 12$; $-12 < k < 12$; $-21 < l < 21$
μ (mm^{-1})	1.806	12.57	0.954	0.970	1.988	0.89	0.99
abs correction	numerical *XSHAPE*[12]	numerical *XSHAPE*[12]	numerical *XSHAPE*[12]	numerical *XSHAPE*[12]	numerical *XSHAPE*[12]	numerical *SADABS*[14]	numerical *SADABS*[14]
transmn	$0.455 < t < 0.816$	$0.041 < t < 0.088$	$0.734 < t < 0.921$	$0.645 < t < 0.868$	$0.817 < t < 0.933$	$0.833 < t < 0.954$	$0.725 < t < 0.902$
R_{int}/R_σ	0.102/0.1752	0.0396/0.0776	0.0261/0.0397	0.1218/0.1328	0.0981/0.0402	0.038/0.038	0.046/0.039
$N(hkl)$ measd; unique	1837; 1009	2001; 1085	6948; 3746	3508; 2035	19451; 2819	3015; 1565	16772; 3663
$N'(hkl)$ [$I > 2\sigma(I)$]	496	631	3105	1323	2796	1501	3653
param refined	88	88	470	236	237	218	362
R values	R1(F) = 0.054, wR2(F^2) = 0.113	R1(F) = 0.035, wR2(F^2) = 0.072	R1 = 0.0345, wR2(F^2) = 0.0663	R1(F) = 0.064, wR2(F^2) = 0.153	R1(F) = 0.0276, wR2(F^2) = 0.0707	R1(F) = 0.028, wR2(F^2) = 0.063	R1(F) = 0.033, wR2(F^2) = 0.080
all data	R1 = 0.142	R1 = 0.088	R1 = 0.0473	R1 = 0.0991	R1 = 0.0279	R1 = 0.029	R1 = 0.033
weighting scheme[15]	0.0247/0	0.0260/0	0.0371/0	0.0739/0	0.0417/0.8691	0.042/0	0/6.7
extinction correction[15]	none	none	0.0020(2)	0.007(2)	0.0121(9)	0.044(3)	none
Flack parameter			0.08(7)	−0.1(2)	0.00(7)	0.03(8)	0.20(9)
residual electron density (max/ min/σ; $e^-/Å^3$)	0.38/−0.45/0.11	0.66/−0.66/0.13	0.69/−0.41/0.09	0.52/−0.46/0.11	0.45/−0.26/0.06	0.40/−0.37/0.08	0.73/−0.48/0.08
comments				nonmerohedral twin	merohedral twin, twin law 010/100/00−1, BASF 0.5113(15)		pseudomerohedral twin, twin law 010/100/00−1, BASF 0.197(2)

dx.doi.org/10.1021/ic400267s | *Inorg. Chem.* 2013, 52, 6011−6020

Table 2. Selected Interatomic Sistances/Å and Angles/deg for $Na_5[B(SO_4)_4]$ (Estimated Standard Deviations in Parentheses)

distances/angles	$Na_5[B(SO_4)_4]$-I	$Na_5[B(SO_4)_4]$-II
Na–O	2.257(4)–2.991(4)	2.262(10)–2.988(10)
S–O^{term}	1.432(3)–1.457(3)	1.404(9)–1.464(8)
S–O^{br}	1.537(3)–1.581(3)	1.535(9)–1.590(7)
B–O	1.444(5)–1.507(5)	1.450(16)–1.488(14)
O^{term}–S–O^{term}	109.4(2)–115.2(2)	110.7(5)–115.3(6)
O^{br}–S–O^{term}	103.2(2)–110.1(2)	100.7(5)–109.1(6)
S–O^{br}–B	126.9(3)–132.6(3)	124.8(8)–139.8(7)
O–B–O	101.1(3)–115.3(4)	103.8(10)–112.5(10)

Table 3. Selected Distances/Å and Angles/deg for $A_3[B(SO_4)_3]$ (A = K, Rb; Estimated Standard Deviations in Parentheses)

distances/angles	$K_3[B(SO_4)_3]$	$Rb_3[B(SO_4)_3]$
M–O	2.746(7)–3.228(9)	2.764(5)–3.214(7)
S1–O^{term}	1.439(7)–1.462(7)	1.438(6)–1.448(6)
S1–O^{br}	1.603(6)	1.591(5)
S2–O^{term}	1.437(7)	1.452(6)
S2–O^{br}	1.519(6)	1.515(6)
B–O4	1.515(9)	1.510(9)
B–O1	1.427(8)	1.440(8)
O^{term}–S–O^{term}	111.7(4)–116.2(3)	112.3(4)–114.8(5)
O^{br}–S–O^{term}	102.9(4)–111.4(3)	102.9(4)–111.2(3)
S–O^{br}–B	125.6(5)–128.9(5)	125.9(4)–129.6(4)
O–B–O	106.4(3)–117.7(10)	106.3(3)–119.2(9)

Table 4. Selected Distances/Å and Angles/deg for $Li[B(S_2O_7)_2]$ and $Li[B(SO_4)_2]$ (Estimated Standard Deviations in Parentheses)

distances/angles	$Li[B(S_2O_7)_2]$	$Li[B(SO_4)_2]$
Li–O	2.047(9)–2.193(10)	1.911(7)–1.979(7)
S–O^{term}	1.376(5)–1.425(4)	1.420(3)–1.429(3)
S–O^{br} (–S)	1.605(5)–1.624(4)	
S–O^{br} (–B)	1.491(4)–1.532(4)	1.517(2)–1.525(2)
B–O	1.433(7)–1.490(9)	1.444(4)–1.472(4)
O^{term}–S–O^{term}	119.7(3)–121.7(3)	116.6(2)–117.38(18)
O^{br}–S–O^{term}	104.0(3)–114.0(3)	106.63(15)–111.42(16)
O^{br}–S–O^{br}	99.1(2)–103.1(2)	97.08(14)–103.44(15)
S–O^{br}–S	120.2(2)–124.7(3)	
S–O^{br}–B	119.9(3)–132.8(4)	127.1(2)–131.8(2)
O–B–O	103.1(4)–114.5(5)	107.0(2)–113.3(3)

located the cations. The A1 positions are between the terminal sulfate anions, and the A2 positions are arranged in ordered zigzag chains between the bridging ones (Figure 5).

In $A_3[B(SO_4)_3]$ (A = K, Rb), also the bond lengths S–O^{br} for the two different sulfur atoms are dissimilar. The bond lengths S–O^{term} range from 1.44 to 1.46 Å (from 1.44 to 1.45 Å for the rubidium compound). The bond length S1–O^{br} is 1.60 Å (1.59 Å) and is significantly longer than S2–O^{br} with 1.52 Å. This situation could be very well compared with the oligosulfates $Pb[S_3O_{10}]$[23] and $(NO_2)_2[S_4O_{13}]$,[24] where the two S^{term}–O^{br} distances are significantly longer than the S^{br}–O^{br} distances. Again, all tetrahedra in $A_3[B(SO_4)_3]$ can be classified as regular [for A = K, BO_4 = 0.58%, S(1)O_4 = 0.11%, S(2)O_4 = 0.55); for A = Rb, BO_4 = 0.65%, S(1)O_4 = 0.14%, S(2)O_4 = 0.76].

The alkali ions are surrounded irregularly 8-fold by oxygen atoms (figure in the SI) with distances between 2.75 and 3.23 Å {2.76–3.21 Å for $Rb[B(SO_4)_3]$}. This distance range agrees well with the sum of the ionic radii; that is, 2.91 Å (CN = 8) for K^+/O^{2-} and 3.00 Å for Rb^+/O^{2-}.[21]

$Li[B(SO_4)_2]$. In a continuation of the building principles of borosulfates, the crystal structure of $Li[B(SO_4)_2]$ consists of a 3D framework of corner-linked tetrahedra with lithium cations in between (Figure 6). Because BO_4 tetrahedra are only connected to SO_4 tetrahedra and vice versa, the 1:2 ratio between boron and sulfur results in a 3D framework. The two symmetry-independent BO_4 tetrahedra are quite similar and regular (B–O = 1.44–1.47 Å; O–B–O = 107–113°). The high regularity results from the 3D framework, where all coordinating SO_4 tetrahedra have the same character. The S–O distances are split into two groups, i.e., longer distances to oxygen atoms connected to BO_4 tetrahedra (1.52–1.53 Å) and shorter ones in coordination to Li^+ (1.42–1.43 Å). This is perfectly in line with the other borosulfates. In general, the deviations from tetrahedral symmetry are small (tables in the SI).

The two independent lithium cations are tetrahedrally coordinated. The distances are quite similar (1.91–1.97 Å) and the tetrahedra remarkably regular (107–113°). All coordinating oxygen atoms come from terminal oxygen atoms of the sulfate anions.

Because all cations show tetrahedral coordination with corner linkage, there is an interesting relation to the structures of SiO_2. As shown in Figure 7, the arrangement of LiO_4, BO_4, and SO_4 tetrahedra is the same that as found in β-tridymite. $Li[B(SO_4)_2]$ represents an ordered variant with a 4-fold enlarged unit cell. The monoclinic *a* axis of $Li[B(SO_4)_2]$ corresponds to the *c* axis of tridymite, and the *bc* plane relates to the orthohexagonal setting of the tridymite unit cell. Deviations from the ideal metrics ($c/b = 0.903 \neq \sqrt{3}/2$) come from the Li/B/S ordering as BO_4 and LiO_4 tetrahedra form parallel zigzag chains in the direction [001] (figures in the SI).

$Li[B(S_2O_7)_2]$. $Li[B(S_2O_7)_2]$ represents the first borosulfate with disulfate groups (Figure 8). According to the composition, the four SO_4 tetrahedra coordinating the central boron atoms come from two disulfate anions. This results in an isolated monoanion $[B(S_2O_7)_2]^-$ (Figure 9). There are two symmetry-different anions with small differences in the orthorhombic low-temperature form. The observed distances and angles correspond to the different topological situations. The B–O distances (1.43–1.49 Å) and O–B–O angles (103–115°) of the BO_4 tetrahedron show more variation than those in $Li[B(SO_4)_2]$ because of the reduced symmetry of the tetrahedral framework. The S–O distances are divided into three groups: short terminal bonds (1.38–1.43 Å), medium bridging bonds to the BO_4 tetrahedron (1.49–1.53 Å), and long bridging bonds of the disulfate unit (1.61–1.62 Å). An analogous behavior is apparent in looking at the angles; i.e., the smallest values are around 100° between bridging oxygen atoms and the highest values around 120° between terminal ones. Again, these findings fit the tendencies in borosulfates, but additionally they are very similar to other disulfate complexes, as described by Wickleder and co-workers.[25]

In contrast to $Li[B(SO_4)_2]$, the Li^+ cations show octahedral surroundings, with enlarged Li–O distances between 2.05 and

dx.doi.org/10.1021/ic400267s | Inorg. Chem. 2013, 52, 6011–6020

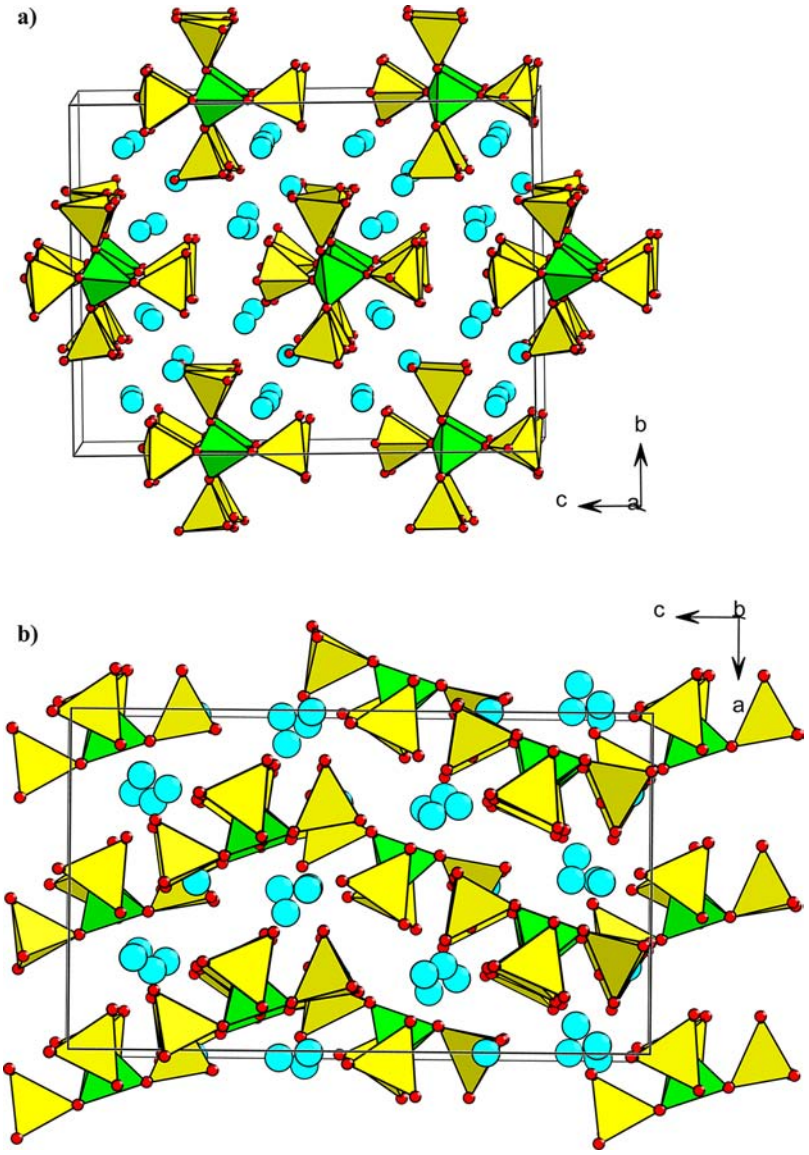

Figure 2. Overview of the unit cell of $Na_5[B(SO_4)_4]$-I: (a) view along [100]; (b) view along [010]. Color code: yellow, SO_4 tetrahedra; green, BO_4 tetrahedra; blue spheres, Na.

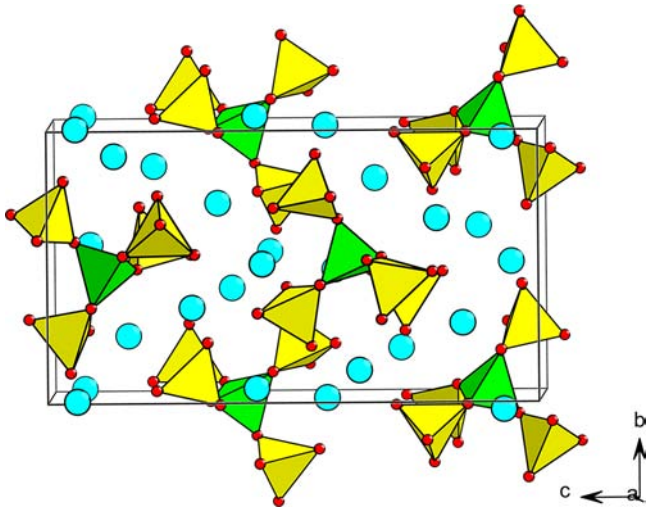

Figure 3. Overview of the unit cell of $Na_5[B(SO_4)_4]$-II: view along [100]. Color code: yellow, SO_4 tetrahedra; green, BO_4 tetrahedra; blue spheres, Na.

2.19 Å (figures in the SI) being well within the expected range based on the sum of the ionic radii. All coordinating oxygen atoms are terminal atoms of the disulfate anions. Interestingly, there are two terminal oxygen atoms of each disulfate group that are not coordinated to lithium (O51 and O61 in Figure 9; additionally O22 and O41).

3.2. Lattice Energies. We checked our structure models for electrostatic reasonability with simple lattice energy calculations using the program *GULP*.[26] The resulting values of the lattice energy (U) are the same as the *MAPLE*[27] values. A comparison with values of chemically similar compounds shows that all of the structures of the novel borosulfates are electrostatically consistent (tables in the SI).

3.3. Vibrational Spectroscopy. The IR and Raman spectra of $K_3[B(SO_4)_3]$, $Na_5[B(SO_4)_4]$-I, $Li[B(SO_4)_2]$, and $Li[B(S_2O_7)_2]$ (figures in the SI) show that the characteristic bands of the tetrahedral BO_4 and SO_4 groups are observed between 1500 and 400 cm^{-1}.[28−36] In general, the number of observed modes is higher for the IR spectra than for the Raman spectra. According to the structural similarity, the spectra of

dx.doi.org/10.1021/ic400267s | *Inorg. Chem.* 2013, 52, 6011−6020

$Na_5[B(SO_4)_4]$-I are nearly identical with those of $K_5[B(SO_4)_4]$ despite the different arrangements of the $[B(SO_4)_4]^-$ anions. Furthermore, there is a closer similarity between $Na_5[B(SO_4)_4]$-I and $K_3[B(SO_4)_3]$ than to the lithium compounds, which deliver higher frequencies. The higher number of modes observed for $K_3[B(SO_4)_3]$ may result from the branched chain because two different types of bridging and terminal S−O bonds occur. Because of the fact that all B−O bonds are bridging ones, we expect the highest frequencies for the terminal S−O modes, i.e., the range between 1150 and 1400 cm^{-1}. Between 400 and 1100 cm^{-1}, the spectra are dominated by the modes of the bridging S−O and B−O bonds. This is in agreement with the literature data for BO_4 and SO_4 tetrahedra[34,35] and the findings of Wickleder et al. for oligosulfates[9,10,24,25] as well.

The assignment in a qualitative manner can be made in analogy to $K_5[B(SO_4)_4]$,[1] which was based on a simulation with the program *VIBRATZ*.[37] Around 1200 cm^{-1}, there are ν_{as}(S−O) vibrations of the SO_4 tetrahedra and, around 1000 cm^{-1}, $\nu_{as}(BO_4)$ modes of the BO_4 tetrahedra. The bending modes $\delta(SO_4)$ and $\delta(BO_4)$ are detected around 500−600 cm^{-1}.

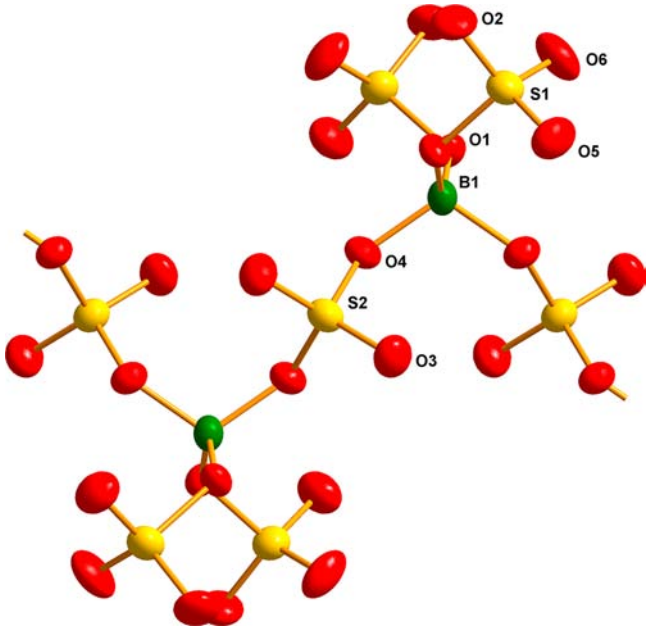

Figure 4. Borosulfate anion in $K_3[B(SO_4)_3]$. Thermal ellipsoids are set to 50% probability.

Because the focus of this contribution is on the synthesis and structural characterization of novel borosulfates, a more detailed discussion of the vibrational spectra will be given in a subsequent publication. It will contain experimental and calculated spectra of further sulfates and borosulfates.[38]

3.4. Thermal Analyses. As pointed out in the Introduction, the thermal behavior of borosulfates is of central interest for the synthesis. Besides the formation by thermally activated evaporation of H_2O and/or SO_3, we expect rearrangements of the tetrahedral framework, changes of the cation's coordination, and decomposition to other solid phases. Figure 10 shows the TGA and DTA measurements of $Na_5[B(SO_4)_4]$-I, $K_3[B(SO_4)_3]$, and $Li[B(S_2O_7)_2]$.

$Na_5[B(SO_4)_4]$-I. Thermal analysis of $Na_5[B(SO_4)_4]$-I shows the evaporation of SO_3 within the temperature range from 707 to 968 K. The detected mass loss of 23.0 wt % corresponds to 1.5 SO_3 molecules per formula unit, as expected for the formation of Na_2SO_4 (theory: 23.5 wt %).

$K_3[B(SO_4)_3]$. From 669 to 1093 K, we see the release of SO_3. The detected mass loss of 28.6 wt % nicely corresponds to 1.5 SO_3 molecules per formula unit, as expected for the formation of K_2SO_4 (theory: 28.8 wt %). Experiments show that the first step is the formation of $K_5[B(SO_4)_4]$. Therefore, we suppose that the two steps proceed as indicated from eqs 3 and 4.

$$K_3[B(SO_4)_3] \rightarrow 0.6K_5[B(SO_4)_4] + 0.6SO_3 + 0.2B_2O_3 \quad (3)$$

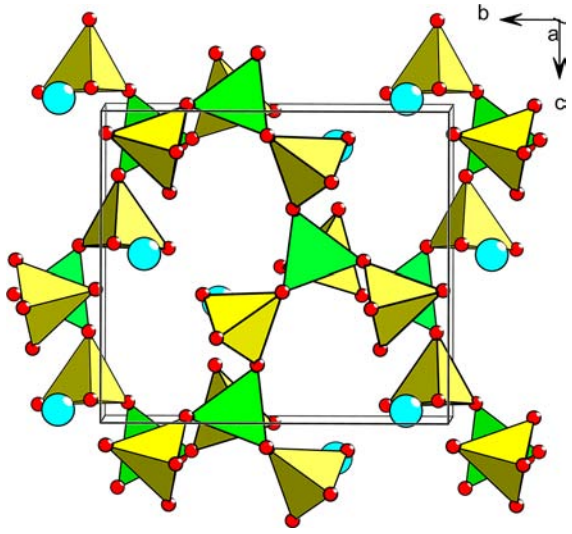

Figure 6. Unit cell of $Li[B(SO_4)_2]$: view along [100]. Color code: yellow, SO_4 tetrahedra; green, BO_4 tetrahedra; blue spheres, Li.

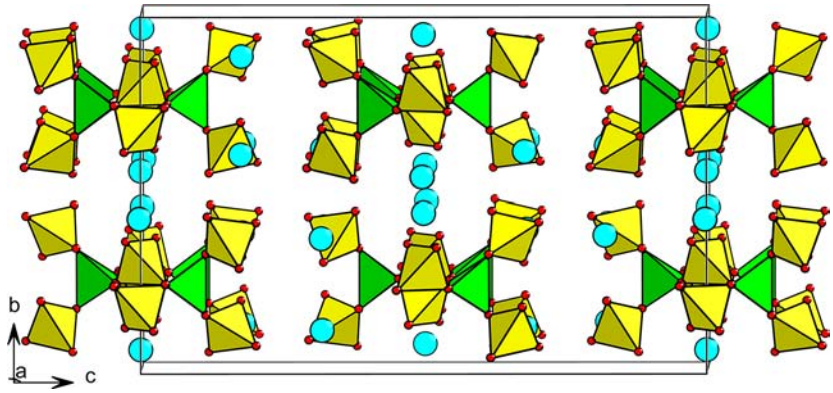

Figure 5. Overview of the unit cell of $K_3[B(SO_4)_3]$ viewed approximately along [100]. Color code: yellow, SO_4 tetrahedra; green, BO_4 tetrahedra; blue spheres, K.

dx.doi.org/10.1021/ic400267s | *Inorg. Chem.* 2013, 52, 6011−6020

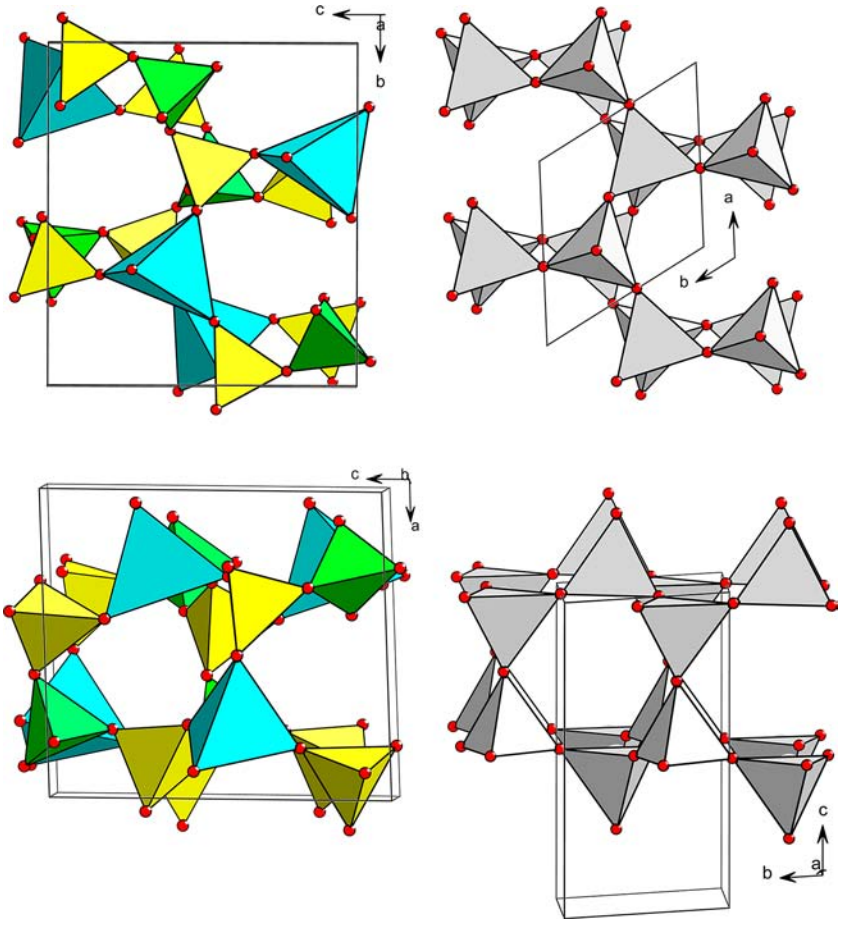

Figure 7. Relationship between $Li[B(SO_4)_2]$ and ß-tridymite. Color code: yellow, SO_4 tetrahedra; green, BO_4 tetrahedra; blue, LiO_4 tetrahedra; gray, SiO_4 tetrahedra.

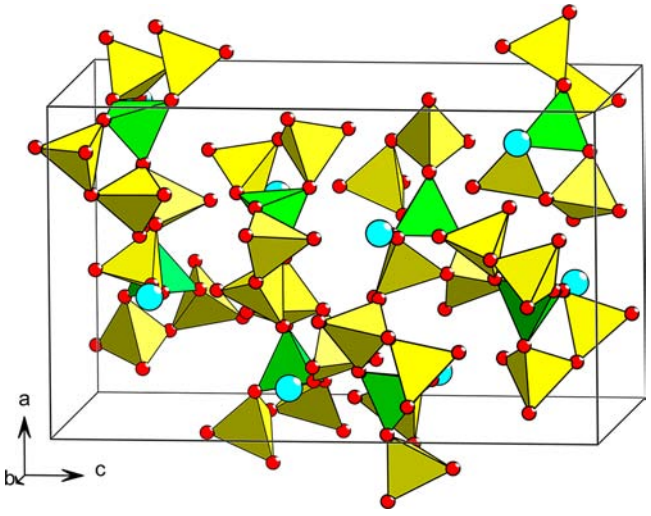

Figure 8. Unit cell of $Li[B(S_2O_7)_2]$. Color code: yellow, SO_4 tetrahedra; green, BO_4 tetrahedra; blue spheres, Li.

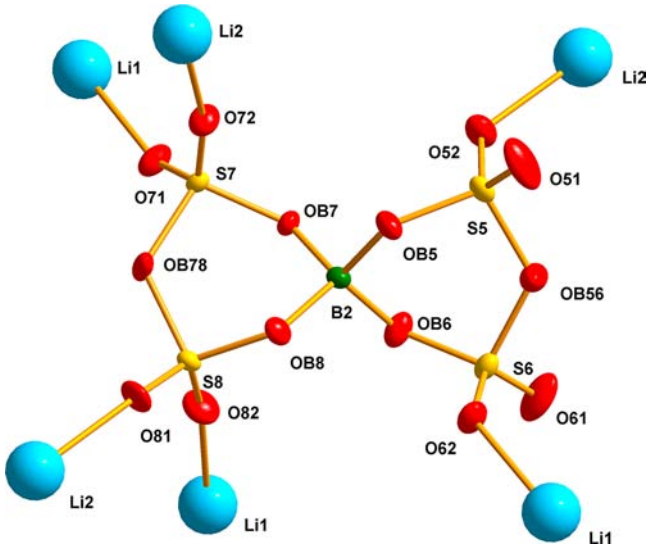

Figure 9. $[B(S_2O_7)_2]^-$ anion in $Li[B(S_2O_7)_2]$. Thermal ellipsoids are set to 50% probability.

$$0.6K_5[B(SO_4)_4] \rightarrow 1.5K_2SO_4 + 0.9SO_3 + 0.3B_2O_3 \quad (4)$$

$Li[B(S_2O_7)_2]$. The decomposition of $Li[B(S_2O_7)_2]$ starts around 350 K. The mass loss of 43.5 wt % up to 530 K indicates the formation of $Li[B(SO_4)_2]$ (theory: 43.2 wt %) according to eq 5. The weight loss continues at 550 K and is nearly completed at 850 K (27.5 wt %). The X-ray pattern of the residue shows the reflections of Li_2SO_4, so a reaction according to eq 6 can be assumed with the formation of amorphous B_2O_3.

$$Li[B(S_2O_7)_2] \rightarrow Li[B(SO_4)_2] + 2SO_3 \quad (5)$$

$$2Li[B(SO_4)_2] \rightarrow Li_2SO_4 + 3SO_3 + B_2O_3 \quad (6)$$

dx.doi.org/10.1021/ic400267s | *Inorg. Chem.* 2013, 52, 6011−6020

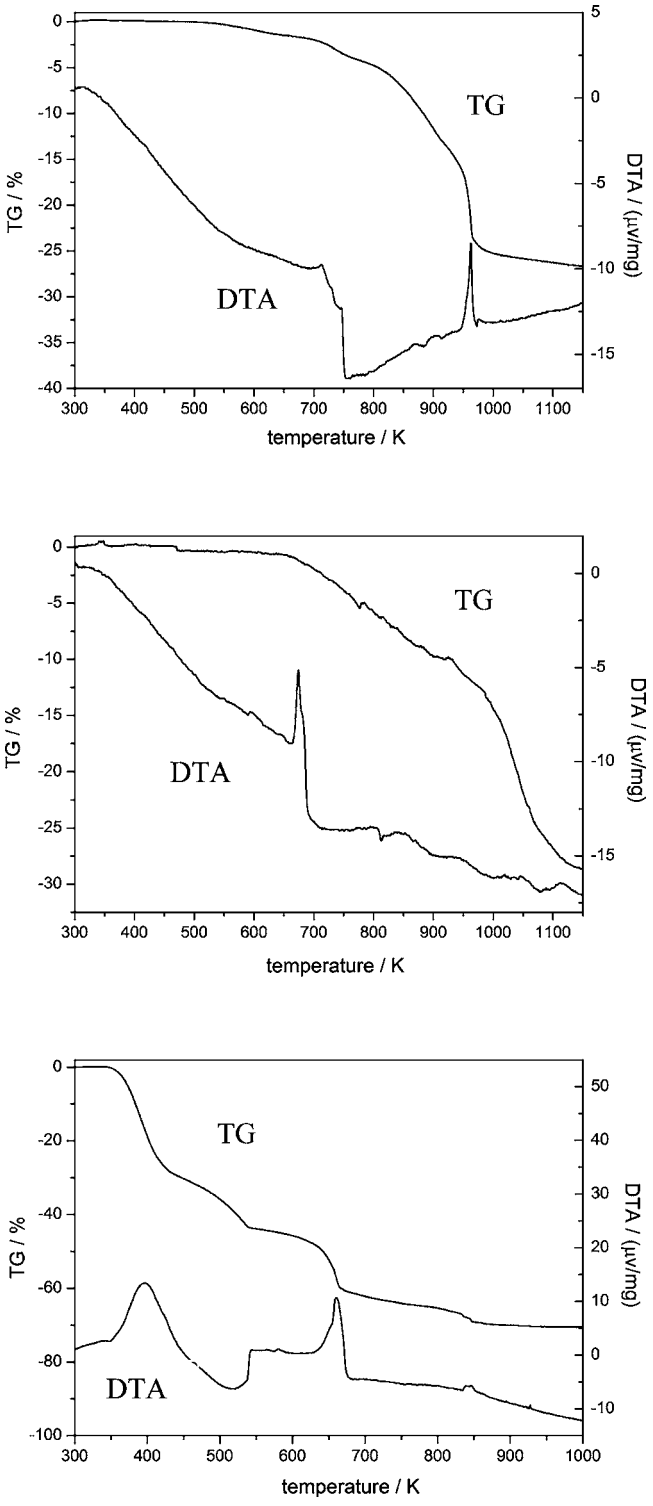

Figure 10. TGA and DTA of $Na_5[B(SO_4)_4]$-I (top) and $K_3[B(SO_4)_3]$ (middle), and $Li[B(S_2O_7)_2)]$ (bottom).

4. CONCLUSIONS

The emphasis of our second publication about borosulfates lies on the systematic exploration of the crystal chemical possibilities that borosulfates may offer. Accordingly, in this contribution, we showed not only the ability for synthesizing further phase-pure borosulfates by variation of the reaction conditions. We also demonstrated the existence of one-dimensional, two-dimensional, and even three-dimensional condensation of the basic tetrahedral building unit $[B(SO_4)_4]$ to form chains and networks, thus an analogy to silicate chemistry. We elucidated the crystal structures of $A_3[B(SO_4)_3]$ (A = K, Rb), $Na_5[B(SO_4)_4]$, and $Li[(B(SO_4)_2]$. The latter was obtained be a well-defined thermal decomposition of $Li[B(S_2O_7)_2]$, the first representative of a borosulfate containing a disulfate group. Additionally, the thermal measurements show us a new way for synthesizing $K_5[B(SO_4)_4]$ by tempering $K_3[B(SO_4)_3]$. We have further undertaken vibrational studies that are similar to those reported for $K_5[B(SO_4)_4]$.

Up to now, all alkali borosulfates contain solely BO_4 tetrahedra that are corner-linked only to SO_4 tetrahedra. This is in contrast to borophosphates, where trigonal-planar BO_3 units and a direct connection of boron polyhedra are observed, a motif that is to be discovered in borosulfate chemistry. On the other hand, we have found the condensation of sulfate to disulfate moieties attached to borate tetrahedra, which is so far not known for borophosphates, where this should, in principle, also be possible. Because both connecting modes may occur simultaneously, the structure chemistry of borosulfates is expected to have a complexity similar to that found for borophosphates.

More detailed investigations on the vibrational spectra might enable assignment of the different connecting modes without determination of the crystal structure, i.e., the occurrence of isolated units ($A_5[B(SO_4)_4]$), chain structures ($A_3[B(SO_4)_3]$), a 3D network ($A[B(SO_4)_2]$), or disulfates ($A[B(S_2O_7)_2]$). This would be of great help in determining structural features in glassy borosulfates. Furthermore, these results may give insight into the structures existing in solution.

Protonated species of borosulfates may represent a special type of complex acid of extraordinary acidity. This high acidity runs parallel with a very low coordination tendency with predominating ionic interactions. Thus, borosulfates are weakly coordinating ions and, therefore, ideal counterions for fluorescent lanthanide ions.[6] Detailed investigations on the physical properties are in progress. Up to now, the majority of borosulfates performs a noncentrosymmetric space group. So, nonlinear optical properties can be expected. The investigation of a new class of compounds is like the discovery of a new "continent" (although maybe small).

■ ASSOCIATED CONTENT

Supporting Information

XRD diagrams, IR and Raman spectra, additional structures, atomic coordinates and displacement parameters deviations from tetrahedral symmetry. This material is available free of charge via the Internet at http://pubs.acs.org.

■ AUTHOR INFORMATION

Corresponding Author

*E-mail: (H.Hö.), harald.hillebrecht@ac.uni-freiburg.de (H.Hi.).

Notes

The authors declare no competing financial interest.

■ REFERENCES

(1) Höppe, H. A.; Kazmierczak, K.; Daub, M.; Förg, K.; Fuchs, F.; Hillebrecht, H. *Angew. Chem.* **2012**, *124*, 6359−6362; *Angew. Chem., Int. Ed.* **2012**, *51*, 6255−6257.
(2) Höppe, H. A. *Solid State Sci.* **2005**, *7*, 1209−1215.
(3) Höppe, H. A.; Daub, M.; Bröhmer, M. C. *Chem. Mater.* **2007**, *19*, 6358−6362.

(4) Mueller-Mach, R.; Mueller, G.; Krames, M. R.; Höppe, H. A.; Stadler, F.; Schnick, W.; Jüstel, T.; Schmidt, P. *Phys. Status Solidi A* **2005**, *202*, 1727−1732.
(5) Chen, M.-Ch.; Li, L.-H.; Chen, Yu-B.; Chen, L. *J. Am. Chem. Soc.* **2011**, *133*, 4617−4624.
(6) (a) Höppe, H. A. *Angew. Chem.* **2009**, *121*, 3626−3636; *Angew. Chem., Int. Ed.* **2009**, *48*, 3572−3582. (b) Jüstel, T.; Nikol, H.; Ronda, C. *Angew. Chem.* **1998**, *110*, 3250−3271; *Angew. Chem., Int. Ed.* **1998**, *37*, 3084−3104 and references cited therein.
(7) Liebau, F. *Structural Chemistry of Silicates*; Springer: Berlin, 1985.
(8) Kniep, R.; Engelhardt, H.; Hauf, C. *Chem. Mater.* **1998**, *10*, 2930−2934.
(9) Betke, U.; Dononelli, W.; Klüner, T.; Wickleder, M. S. *Angew. Chem.* **2011**, *123*, 12569−12571; *Angew. Chem., Int. Ed.* **2011**, *50*, 12361−12363.
(10) Logemann, C.; Klüner, T.; Wickleder, M. S. *Chem.—Eur. J.* **2011**, *17*, 758−760.
(11) Mumme, W. G. *Acta Crystallogr., Sect. B* **1973**, *29*, 1076−1083.
(12) Stoe & Cie (Darmstadt), Programs *X-RED* and *X-SHAPE*, 1999−2011.
(13) Remove, T. *SAINT, Data reduction and frame integration program for the CCD area-detector system*; Bruker Analytical X-ray Systems: Madison, WI, 2006.
(14) Sheldrick, G. M. *SADABS, Program for area detector adsorption correction*; Institute for Inorganic Chemistry, University of Göttingen: Göttingen, Germany, 1996.
(15) Sheldrick, G. M. *SHELXTL*, version 5.10; Crystallographic System, Bruker AXS Analytical X-ray Instruments Inc.: Madison, WI, 1997.
(16) Spek, A. L. *PLATON—A Multipurpose Crystallographic Tool*; Utrecht University: Utrecht, The Netherlands, 2008. Windows implementation: Farrugia, L. J. University of Glasgow, Glasgow, Scotland, 2008.
(17) (a) Kniep, R.; Gçzel, G.; Eisenmann, B.; Röhr, C.; Asbrand, N.; Kizilyalli, M. *Angew. Chem.* **1994**, *106*, 791−793; *Angew. Chem., Int. Ed. Engl.* **1994**, *33*, 749−751.
(18) Balic-Zunic, T.; Makovicky, E. *Acta Crystallogr., Sect. B* **1996**, *52*, 78−81.
(19) Makovicky, E.; Balic-Zunic, T. *Acta Crystallogr., Sect. B* **1998**, *54*, 766−773.
(20) Höppe, H. A. *J. Solid State Chem.* **2009**, *182*, 1786−1791. Huang, Y.; Kniep, R. *Z. Anorg. Allg. Chem.* **2007**, *633*, 1517−1540.
(21) Shannon, R. D. *Acta Crystallogr., Sect. A* **1976**, *32*, 751−767.
(22) Brown, I. D. *J. Appl. Crystallogr.* **1996**, *29*, 479−480.
(23) Logemann, C.; Klüner, T.; Wickleder, M. S. *Z. Anorg. Allg. Chem.* **2012**, *638*, 758−762.
(24) Logemann, C.; Klüner, T.; Wickleder, M. S. *Angew. Chem.* **2012**, *124*, 5082−5085; *Angew. Chem., Int. Ed.* **2012**, *51*, 4997−5000.
(25) (a) Logemann, C.; Wickleder, M. S. *Inorg. Chem.* **2011**, *50*, 11111−11116. (b) Bruns, J.; Eul, M.; Pöttgen, R.; Wickleder, M. S. *Angew. Chem.* **2012**, *124*, 2242−2246; *Angew. Chem., Int. Ed.* **2012**, *51*, 2204−2207.
(26) (a) Gale, J. D. *J. Chem. Soc., Faraday Trans.* **1997**, *1*, 629. (b) Gale, J. D.; Rohl, A. L. *Mol. Simul.* **2003**, *29*, 291.
(27) (a) Hoppe, R. *Angew. Chem.* **1966**, *78*, 52−63; *Angew. Chem. Int. Ed. Engl.* **1966**, *5*, 95−106. (b) Hoppe, R. *Angew. Chem.* **1970**, *82*, 7−16; *Angew. Chem., Int. Ed. Engl.* **1970**, *9*, 25−34. (c) Hübenthal, R. *MAPLE, Program for the Calculation of the Madelung Part of Lattice Energy*; University of Gießen: Gießen, Germany, 1993.
(28) Tanaka, K.; Naruse, H.; Morikawa, H.; Marumo, F. *Acta Crystallogr., Sect. B* **1991**, *47*, 581−588.
(29) Pascard, R.; Pascard-Billy, C. *Acta Crystallogr.* **1965**, *18*, 830−834.
(30) Gurr, G. E.; Montgomery, P. W.; Knutson, C. D.; Gorres, B. T. *Acta Crystallogr., Sect. B* **1970**, *26*, 906−915.
(31) Ståhl, K.; Balic-Zunic, T.; da Silva, F.; Eriksen, K. M.; Berg, R. W.; Fehrmann, R. *J. Solid State Chem.* **2005**, *178*, 1697−704.
(32) Touzain, P.; Brisse, F.; Caillet, M. *Can. J. Chem.* **1970**, *48*, 3358−3361.
(33) Touzain, P.; Caillet, M. *Rev. Chim. Miner.* **1971**, *8*, 277−286.
(34) Jun, L.; Shuping, X.; Shiyang, G. *Spectrochim. Acta, Part A* **1995**, *51*, 519−532.
(35) Kloprogge, J. T.; Ruan, H.; Duong, L. V.; Frost, R. L. *Neth. J. Geosci.* **2001**, *80*, 41−47.
(36) Jun, L.; Shuping, X.; Shiyang, G. *Spectrochim. Acta, Part A* **1995**, *51*, 519−532.
(37) Program *VIBRATZ V2.2*: Dowty, E. *Chem. Phys. Miner.* **1987**, *14*, 67.
(38) Daub, M.; Höppe, H.; Hillebrecht, H., publication in preparation.